Eur. Phys. J. E (2012) **35**: 13
DOI 10.1140/epje/i2012-12013-2

THE EUROPEAN PHYSICAL JOURNAL E

Regular Article

Effect of salt on the compression of polyelectrolyte brushes in a theta solvent

M.W. Matsen[a]

School of Mathematical and Physical Sciences, University of Reading, Whiteknights, Reading RG6 6AX, UK

Received 24 November 2011 and Received in final form 5 February 2012
Published online: 27 February 2012 –

Abstract. Classical strong-stretching theory (SST) predicts that, as opposing polyelectrolyte brushes are compressed together in a salt-free theta solvent, they contract so as to maintain a finite polymer-free gap, which offers a potential explanation for the ultra-low frictional forces observed in experiments despite the application of large normal forces. However, the SST ignores chain fluctuations, which would tend to close the gap resulting in physical contact and in turn significant friction. In a preceding study, we examined the effect of fluctuations using self-consistent field theory (SCFT) and illustrated that high normal forces can still be applied before the gap is destroyed. We now look at the effect of adding salt. It is found to reduce the long-range interaction between the brushes but has little effect on the short-range part, provided the concentration does not enter the salted-brush regime. Consequently, the maximum normal force between two planar brushes at the point of contact is remarkably unaffected by salt. For the crossed-cylinder geometry commonly used in experiments, however, there is a gradual reduction because in this case the long-range part of the interaction contributes to the maximum normal force.

1 Introduction

It has been nearly two decades since 1994 when Klein *et al.* [1] discovered that polymer brushes are remarkably effective at reducing the friction between sliding surfaces. The latest revelation came in 2003, when Raviv *et al.* [2] showed that the friction is even lower for polyelectrolyte brushes. Indeed subsequent experiments on the same system [3] as well as a different system [4] have reconfirmed the ultra-low frictional forces, but only for strong (quenched) polyelectrolyte brushes. Liberelle and Giasson [5] found the friction between weak (annealed) polyelectrolyte brushes to be similar to that of neutral brushes.

The main source of friction is understood to be the collisions between polymer chains from the two opposing brushes [2–4, 6–10]. It has been suggested that charged polymers slide past each other more easily because they are surrounded by hydration layers [2–4]. Furthermore, it is thought that the interpenetration and hence the number of collisions is less between polyelectrolyte brushes than between neutral brushes under equivalent loads (*i.e.*, normal forces), because polyelectrolyte brushes remain further apart on account of the osmotic pressure from the counter ions [2–4]. Indeed, simulations [11–13] have found that there is less interpenetration between polyelectrolyte brushes. Interestingly though, the simulations also found that polyelectrolyte brushes seem to contract more under compression than their neutral counterparts, which further reduces the amount of interpentration.

As it turns out, Zhulina and Borisov [14] had already predicted in 1997 that polyelectrolyte brushes contract, in fact, sufficiently enough to always maintain a polymer-free gap when compressed together in a salt-free theta solvent. Their prediction was derived from an exact analytical solution of the strong-stretching theory (SST) derived by Semenov [15] and by Milner, Witten and Cates [16]. The contraction occurs because the reduction in volume available to the counter ions outside the brushes reduces their translational entropy. As a result, the ions are pulled back into the brushes where they screen the electrostatic interactions, allowing the brushes to relax. Although, strictly speaking, the SST calculation is for static equilibrated brushes, this mechanism will continue to operate in the presence of shear. In fact, we can expect the equilibrium calculation to remain reasonably accurate so long as there is a finite gap separating the opposing brushes.

The SST prediction suggests that the superb performance of polyelectrolyte brushes occurs because the normal force is able to increase as the brushes are compressed together, while the gap simultaneously prevents any significant sliding friction. However, the prediction of a polymer-free gap will eventually break down. This is because SST ignores chain fluctuations which produce tails that extend beyond the classical brush profiles, reducing the width of the polymer-free gap. In a previous study [17],

[a] e-mail: m.w.matsen@reading.ac.uk

we illustrated that these tails are particularly large for polyelectrolyte brushes, bringing into question the actual effectiveness of the polymer-free gap. We then proceeded to investigate the impact of chain fluctuations using the self-consistent field theory (SCFT) of Edwards [18]. Ultimately, our study illustrated that the gap should survive fluctuations long enough for the system to acquire a substantial normal force before contact occurs.

Not surprisingly perhaps, biological systems seem to take advantage of this mechanism for producing low friction, in particular on the cartilage surfaces of mammalian joints [19]. Indeed this mechanism is being considered in the design of artificial joints [20]. In vivo, however, there is a significant salt concentration [21], which would tend to screen the electrostatic interactions. Fortunately, preliminary studies [2,3] indicate that the ultra-low frictional forces between strong polyelectrolyte brushes do survive significant levels of salt. Here we now extend our previous SST and SCFT calculations [17] to investigate the effect of salt on the polymer-free gap between compressed polyelectrolyte brushes.

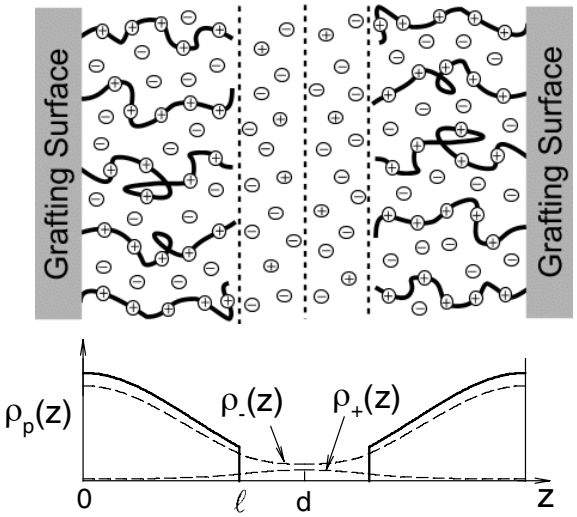

Fig. 1. Schematic diagram of opposing polyelectrolyte brushes compressed together, along with a schematic plot of the polymer profile $\rho_p(z)$ (solid curves) and the positive and negative ion distributions $\rho_\pm(z)$ (dashed curves).

2 Theory

We consider two identical opposing polyelectrolyte brushes compressed to a separation of $2d$ in a salt solution of concentration ρ_s (see fig. 1). Each brush has a grafting density of $\sigma \equiv n_p/A$, where n_p is the number of grafted chains and A is the area of the grafting surface. The chains are monodisperse with a natural end-to-end length of $R_0 \equiv aN^{1/2}$, where N is the number of segments per chain and a is the statistical segment length. Furthermore, each chain has N_c ionic units distributed along its backbone with all the counter ions dissociating into the salt solution (*i.e.*, a quenched polyelectrolyte). The resulting charge on the polymer is taken to be positive and is smeared uniformly along the polymer backbone, which is a valid approximation provided that $N_c \gg 1$. The average segment concentration, $\rho_p(z)$, is assumed to be semi-dilute relative to the melt concentration, ρ_0, which allows us to integrate out the solvent coordinates so as to treat the solvent implicitly. The integration combines the solvent interactions and translational entropy of the solvent into an excluded-volume parameter, v, which is set to zero for a theta solvent [22]. The positive and negative ions, which are assumed to be monovalent with charge $\pm e$, are treated explicitly in the grand-canonical ensemble with their concentrations denoted by $\rho_\pm(z)$. The strength of the electrostatic interactions is specified by the usual Bjerrum length, $\ell_B = e^2/4\pi\epsilon k_B T$, where ϵ is the electric permittivity of the solvent.

To simplify the problem, we work in terms of dimensionless quantities and reduced parameters. Most lengths are divided by R_0 to produce, for example, the dimensionless coordinate, $Z \equiv z/R_0$, and the dimensionless separation, $D \equiv d/R_0$. The dimensionless Bjerrum length, however, is defined as

$$L_B \equiv 4\pi\ell_B\sigma R_0, \tag{1}$$

so as to scale the grafting density, σ, out of the problem. With this in mind, we define the dimensionless polymer concentration as

$$\Phi_p(Z) \equiv \frac{R_0}{\sigma N}\rho_p(z), \tag{2}$$

which is normalized such that $\int \Phi_p(Z)\mathrm{d}Z = 1$. Similarly, the dimensionless ion concentrations are

$$\Phi_\pm(Z) \equiv \frac{R_0}{\sigma N_c}\rho_\pm(z). \tag{3}$$

The electrostatic potential, $\psi(z)$, is converted to the usual dimensionless potential,

$$\Psi(Z) \equiv \frac{e}{k_B T}\psi(z). \tag{4}$$

In terms of scaled quantities, the Poisson-Boltzmann equation (or equivalently, the Maxwell equation) becomes

$$\Psi''(Z) = -L_B N_c[\Phi_p(Z) - \Phi_-(Z) + \Phi_+(Z)], \tag{5}$$

where the ion concentrations are given by

$$\Phi_\pm(Z) = \Phi_s \exp(\mp\Psi(Z)). \tag{6}$$

In the grand-canonical ensemble, the concentrations would normally involve chemical potentials in addition to the electrostatic potential. However, both chemical potentials can be set to zero by adjusting the electrostatic potential so that $\Psi(Z) \to 0$ in the coexisting salt solution, and including the prefactor, $\Phi_s \equiv \rho_s R_0/\sigma N_c$, which is interpreted as a dimensionless bulk salt concentration.

2.1 SST treatment

In the strong-stretching theory (SST), the brush has a well-defined height, ℓ, from which we define $L = \ell/R_0$

(see fig. 1). This allows us to separate the system into two distinct regions, for which the boundary conditions of the Poisson-Boltzmann equation are [17]

$$\Psi'(0) = 0, \tag{7}$$

$$\Psi'(L) = -L_B N_c(1 - f_c), \tag{8}$$

$$\Psi'(D) = 0. \tag{9}$$

The quantity

$$f_c \equiv \int_0^L [\Phi_-(Z) - \Phi_+(Z)]\mathrm{d}Z \tag{10}$$

defines the degree to which the polymer brush is screened by the free ions.

Firstly, we solve the interior region, $0 \leq Z \leq L$, containing the polymer. As argued by Milner, Witten and Cates [16], the field, $w(z)$, acting on the polymer is generally parabolic. If we then assume a theta solvent where the polymers only feel the electrostatic field (*i.e.*, $w(z) \propto \psi(z)$), it follows that [14,17,23]

$$\Psi(Z) = \frac{3\pi^2}{8N_c}(L^2 - Z^2) + \Psi_L, \tag{11}$$

where Ψ_L is a constant that needs to be determined. From this, the Poisson-Boltzmann eq. (5) implies a polymer concentration of

$$\Phi_p(Z) = \Phi_-(Z) - \Phi_+(Z) + \frac{3\pi^2}{4L_B N_c^2}, \tag{12}$$

which immediately yields

$$f_c = 1 - \frac{3\pi^2 L}{4L_B N_c^2}. \tag{13}$$

By substituting eqs. (6) and (11) into eq. (10), we obtain one further condition

$$f_c = 2\Phi_s \int_0^L \sinh\left(\frac{3\pi^2}{8N_c}(L^2 - Z^2) + \Psi_L\right)\mathrm{d}Z. \tag{14}$$

Secondly, we solve the Poisson-Boltzmann eq. (5) for the exterior region, $L \leq Z \leq D$. By setting $\Phi_p(Z) = 0$, the equation reduces to

$$\Psi''(Z) = 2L_B N_c \Phi_s \sinh(\Psi(Z)), \tag{15}$$

from which it follows that the electric potential decays to zero with a characteristic distance equal to the usual Debye screening length

$$\lambda_\mathrm{D} \equiv \Lambda_\mathrm{D} R_0 = \frac{R_0}{\sqrt{2L_B N_c \Phi_s}}. \tag{16}$$

The first step in solving eq. (15) is to multiply by $\Psi'(Z)$ and integrate, which gives

$$\frac{1}{2}[\Psi'(Z)]^2 = 2L_B N_c \Phi_s[\cosh(\Psi(Z)) - \cosh(\Psi_D)], \tag{17}$$

where the integration constant is chosen so as to satisfy the boundary condition at D, eq. (9). The remaining boundary condition at L, eq. (8), is then satisfied by requiring

$$L_B N_c(1 - f_c)^2 = 4\Phi_s[\cosh(\Psi_L) - \cosh(\Psi_D)]. \tag{18}$$

One further relation relating Ψ_L and Ψ_D is required, and this is obtained by integrating eq. (17) to give

$$\int_{\Psi_D}^{\Psi_L} \frac{\mathrm{d}\Psi}{\sqrt{\cosh(\Psi) - \cosh(\Psi_D)}} = 2\sqrt{L_B N_c \Phi_s}(L - D). \tag{19}$$

Once f_c, L, ψ_L and ψ_D have been determined, we can then calculate the free energy of each brush, which is conveniently divided into three parts, $F(D) = F_p + F_c + F_e$. The entropic stretching energy, F_p, of the polymer chains is given by

$$\frac{F_p}{n_c k_B T} = \frac{3\pi^2}{8N_c}\int_0^L Z^2 \Phi_p(Z)\mathrm{d}Z, \tag{20}$$

$$= \Psi(0) - \int_0^L \Phi_p(Z)\Psi(Z)\mathrm{d}Z, \tag{21}$$

where $n_c = N_c n_p$. Equation (20) comes from a well-known expression developed by Milner, Witten and Cates [16], and the equivalence to eq. (21) is an immediate consequence of the fact $Z^2 \propto \Psi(0) - \Psi(Z)$. The translational entropy, F_c, of the counter ions is

$$\frac{F_c}{n_c k_B T} = \int_0^D [\Phi_-(Z)\ln(\Phi_-(Z)/\Phi_s) + \Phi_+(Z)\ln(\Phi_+(Z)/\Phi_s)]\mathrm{d}Z, \tag{22}$$

$$= \int_0^D [\Phi_-(Z) - \Phi_+(Z)]\Psi(Z)\mathrm{d}Z. \tag{23}$$

Finally, the electrostatic energy, F_e, is

$$\frac{F_e}{n_c k_B T} = \frac{1}{2}\int_0^D \Psi(Z)[\Phi_p(Z) - \Phi_-(Z) + \Phi_+(Z)]\mathrm{d}Z, \tag{24}$$

$$= \frac{1}{2L_B N_c}\int_0^D [\Psi'(Z)]^2\mathrm{d}Z, \tag{25}$$

$$= \frac{3\pi^4 L^3}{128 L_B N_c^3} + \sqrt{\frac{\Phi_s}{L_B N_c}} \times \int_{\Psi_D}^{\Psi_L} \sqrt{\cosh(\Psi) - \cosh(\Psi_D)}\mathrm{d}\Psi. \tag{26}$$

The transformation from eq. (24) to eq. (25) is achieved using the Poisson-Boltzmann eq. (5) with integration by parts, and then eq. (26) follows from eqs. (11) and (17).

Summing up the three contributions, the total free energy of each brush reduces to

$$\frac{F(D)}{n_c k_B T} = \Psi(0) - \frac{F_e}{n_c k_B T}. \tag{27}$$

The compression force between two parallel plates separated by a distance of $2D$ (in units of $R_0 = aN^{1/2}$) is then evaluated using

$$\text{force} = -F'(D)/R_0. \tag{28}$$

In practice however, it is extremely challenging to construct well-aligned flat surfaces unless they are somewhat deformable as with biological systems [19], but then it would be difficult to perform systematic studies. Therefore, experiments [1–5] generally measure the force between two identical crossed cylinders. Provided that the radius, R, of the cylinders is large, the Derjaguin approximation [24–26] estimates the force as

$$\text{force} \approx 4\pi\sigma R[F(D) - F(\infty)]/n_p, \tag{29}$$

where $2D$ now represents the minimum distance between the crossed cylinders.

2.2 SCFT treatment

In order to investigate the effect of chain fluctuations, we also perform calculations using self-consistent field theory (SCFT) [27–29]. The SCFT calculation mirrors that of SST, except that the polymer concentration is given by

$$\Phi_p(Z) = \frac{1}{q(\Delta,1)}\int_0^1 q(Z,s)q^\dagger(Z,s)\mathrm{d}s, \tag{30}$$

where $q(Z,s)$ satisfies the modified diffusion equation,

$$\frac{\partial}{\partial s}q(Z,s) = \Big[\frac{1}{6}\frac{\partial^2}{\partial Z^2} - w(Z)\Big]q(Z,s), \tag{31}$$

subject to the initial condition $q(Z,0) = 1$. Similarly, $q^\dagger(Z,s)$ satisfies an analogous diffusion equation but with the right-hand side multiplied by -1. Again it is solved with the same boundary conditions, but subject to the condition $q^\dagger(Z,1) = \delta(Z-\Delta)$, where Δ is a small positive constant (*e.g.*, 10^{-4}). Note that it is very important that Δ is kept fixed throughout the calculation [17,26].

So as to prevent the polymers from penetrating the grafting surface, the diffusion equation is solved with the Dirichlet boundary condition at $Z = 0$ (*e.g.*, $q(0,s) = 0$) [30,31]. Using the symmetry about the midplane, the diffusion equation is solved over the interval $0 \le Z \le D$ with the Neumann boundary condition (*e.g.*, $\frac{\partial}{\partial Z}q(D,s) = 0$). In cases where D is much larger than the height of the brush, it is sufficient to solve the diffusion equation over the smaller interval, $0 \le Z \le L$, where $L < D$ is chosen large enough that $\Phi_p(L)/\Phi_p(0) < 10^{-9}$.

A numerical solution of SCFT begins with an initial guess for $w(Z)$. For this, we use either the SST solution or a previous SCFT solution obtained for a neighboring set of parameter values. Next the diffusion eq. (31) is solved on a discrete mesh by the standard Crank-Nicolson algorithm [32]. Once $\Phi_p(Z)$ has been evaluated, $\Psi(Z)$, is determined by solving the Poisson-Boltzmann eq. (5) using the Newton-Raphson algorithm, which is particularly fast as the Jacobian is tridiagonal. Next the field is adjusted to satisfy $w(Z) = N_c\Psi(Z)$ using the Anderson-mixing scheme [33]; convergence is generally achieved within just 20 iterations. If $L = D$ then the calculation is performed with $f_c = 1$, but otherwise f_c is adjusted by a Newton-Raphson iteration so as to satisfy eq. (14). Even though we use a very fine mesh in order to achieve high precision (*e.g.*, 5000 points along the chain contour and 4000 spatial points for $0 < Z < L$), a self-consistent solution takes less than a minute to evaluate on a single CPU.

Once the self-consistent solution is obtained, the entropic stretching energy, F_p, of the brush is given by

$$\frac{F_p}{n_c k_B T} = -\frac{1}{N_c}\ln q(\Delta,1) - \int_0^D \Phi_p(Z)\Psi(Z)\mathrm{d}Z, \tag{32}$$

where $n_c = N_c n_p$. The entropic translational energy, F_c, of the counter ions and the electrostatic energy, F_e, are still given by eqs. (23) and (24), respectively.

By applying a reflecting boundary condition at $Z = D$, the polymer concentration, $\Phi_p(Z)$, will automatically be a mixture of the two brushes. Nevertheless it is straightforward to extract the concentration, $\Phi_{p0}(Z)$, of the single brush grafted to $Z = \Delta$. This is done by reflecting $w(Z)$ about the midplane, and solving the diffusion eq. (31) in the full interval, $0 \le Z \le 2D$, with Dirichlet boundary conditions and the same initial conditions as above. The resulting polymer concentration will then be $\Phi_{p0}(Z)$, and from that we can evaluate the degree of interpenetration between the opposing brushes by

$$\Sigma_p = \int_D^{2D} \Phi_{p0}(Z)\mathrm{d}Z. \tag{33}$$

Strictly speaking, there will always be some overlap between the opposing brushes for any finite D (*i.e.*, $\Sigma_p > 0$), although it may be extremely small. For practical purposes, however, we will follow our earlier study [17] and define the point of physical contact between the brushes by the criterion $\Sigma_p = 0.01$.

3 Results

Although the system has been greatly simplified with the appropriate choice of dimensionless quantities, there still remains four separate control parameters: N_c, L_B, Φ_s and D. In the SST, however, N_c can be scaled out of the problem by dividing all lengths by $N_c^{1/2}$ and multiplying all concentrations by $N_c^{1/2}$, which reduces the number of control parameters to three: $L_B N_c^{3/2}$, $\Phi_s N_c^{1/2}$ and $D/N_c^{1/2}$. Even still, this is a large parameter space and therefore we limit our calculations to $L_B N_c^{3/2} = 100$, which is just inside the osmotic regime where the charge on the polymer is largely screened by the free ions [17]. In the SCFT, the choice of N_c controls the level of chain fluctuations, which we will illustrate by comparing results for $N_c = 25$ and 100.

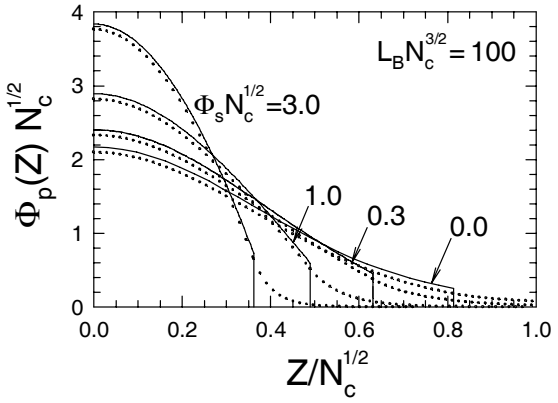

Fig. 2. SST predictions for the polymer profile of an isolated brush, $\Phi_p(Z)$, plotted for different salt concentrations, Φ_s. The dotted curves show the net negative charge from the free ions, $\Phi_-(Z) - \Phi_+(Z)$, screening the positive charge of the polymer.

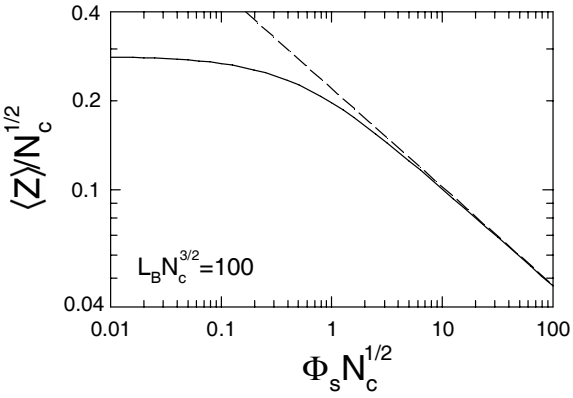

Fig. 3. SST prediction for the average segment height of an isolated brush, $\langle Z \rangle$, as a function of salt concentration, Φ_s. The dashed line, obtained by combining $\langle Z \rangle = 3L/8$ with eq. (35), demonstrates the $\langle Z \rangle \sim \Phi_s^{-1/3}$ scaling in the salted-brush regime.

3.1 SST for an isolated brush

The isolated brush (*i.e.*, $D \to \infty$ and $\Psi_D = 0$) has already been solved by Zhulina and Borizov [23], but with a different choice of reduced parameters [34]. For this simple case, we have just two parameters, $\Phi_s N_c^{1/2}$ and $L_B N_c^{3/2}$, the latter of which is fixed at 100. Once the parameters have been chosen, the SST solution is obtained by solving eq. (14) for f_c, with L and Ψ_L expressed as functions of f_c using eqs. (13) and (18), respectively.

Figure 2 shows the polymer profile (solid curves) for a series of salt concentrations, Φ_s. As the salt concentration increases, the brush contracts and gradually acquires a parabolic shape,

$$\Phi_p(Z) \approx \Phi_s \frac{3\pi^2}{4N_c}(L^2 - Z^2), \tag{34}$$

where the brush height decreases as

$$L \approx \left(\frac{2N_c}{\pi^2 \Phi_s}\right)^{1/3}. \tag{35}$$

The dotted curves in fig. 2 show the net negative charge from the free ions, $\Phi_-(Z) - \Phi_+(Z)$. It closely tracks the polymer concentration, $\Phi_p(Z)$, inside the brush and then decays to zero outside the brush. The decay coincides with the Debye screening lengths, $\Lambda_D/N_c^{1/2} = 0.0408$, 0.0707 and 0.1291 calculated for $\Phi_s N_c^{1/2} = 3.0$, 1.0 and 0.3, respectively. The decay for the zero-salt limit is given by the Gouy-Chapman length, $\Lambda_{GC}/N_c^{1/2} = 0.3322$ [17].

Figure 3 examines the contraction of the brush by plotting the average segment height, $\langle Z \rangle \equiv \int Z \Phi_p(Z) \mathrm{d}Z$, as a function of salt concentration. The dashed line demonstrates the $\langle Z \rangle \sim \Phi_s^{-1/3}$ scaling that occurs at high salt concentrations, referred to as the salted-brush regime. It is obtained by combining the result $\langle Z \rangle = 3L/8$ for the parabolic profile in eq. (34) with the approximate height in eq. (35). This behavior of $\langle Z \rangle$ predicted by SST is indeed nicely consistent with experiment [35]. Simulations [36,37] have also found a similar scaling exponent, although it is for the decrease in brush height as a function of the average concentration of ions inside the brush as opposed to the bulk salt concentration, Φ_s, far from the brush.

3.2 SCFT for an isolated brush

Now we examine the effect of chain fluctuations on the isolated brush using SCFT. Figure 4a starts by comparing the polymer profiles for $N_c = 25$ (dashed curves) and $N_c = 100$ (solid curves) to those predicted by SST (dotted curves) from fig. 2. The fluctuations have two main effects [32]; firstly they cause a depletion zone next to the substrate, and secondly they create a tail that extends beyond the classical brush height, L. Nevertheless, for intermediate values of Z, the SCFT profiles match the SST prediction very well, although the agreement starts to degrade for large Φ_s on account of the fact the chains are less stretched.

For neutral brushes, the height of the tail scales as $L^{-1/3}$ [32,38]. However, our previous study [17] for polyelectrolyte brushes in a salt-free solvent showed that the tail deviates from this conventional scaling because the self-consistent field, $w(Z)$, remains smooth at the brush edge. Nevertheless there is a discontinuity in the second derivative of $w(Z)$ proportional the sudden drop in polymer concentration, $\Phi_p(L)$. As a consequence, the characteristic height of the tail is instead given by

$$\xi \equiv \Xi R_0 = \frac{L^{1/5} R_0}{(L_B N_c^2 \Phi_p(L))^{2/5}}. \tag{36}$$

According to eq. (5), the discontinuity in the second derivative of $w(Z) = N_c \Psi(Z)$ does not depend on Φ_s, and thus we might expect the same scaling to hold, but the scaling plot in fig. 4b illustrates that this is not the case. The reason is that the derivation of eq. (36) assumes the charge distribution from the free ions, $\Phi_-(Z) - \Phi_+(Z)$, is approximately linear over the range of the tail, whereas

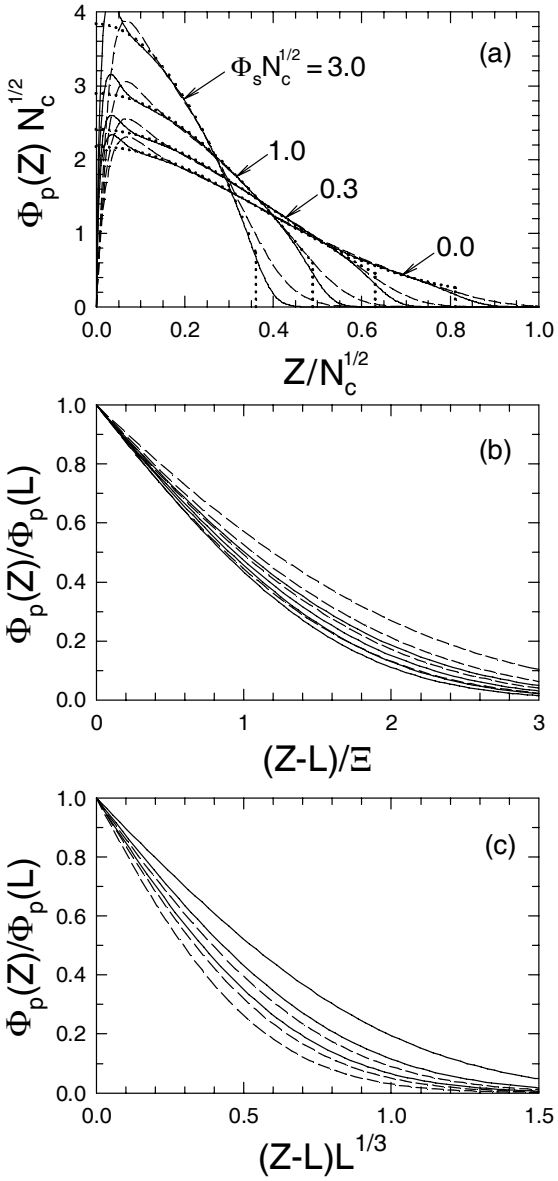

Fig. 4. (a) SCFT predictions for the polymer profile of an isolated brush, $\Phi_p(Z)$, plotted for different salt concentrations, Φ_s. The dashed and solid curves are for brushes with $N_c = 25$ and 100 charges per polymer chain, while the dotted curves show the SST predictions from fig. 2. Plots (b) and (c) show the tails scaled with Ξ from eq. (36) and $L^{-1/3}$, respectively.

fig. 2 shows that this is no longer true even for small amounts of salt. If the salt concentration was large enough, however, the field would quickly drop to zero outside the brush much the same as it does for neutral brushes, and thus we could expect the conventional $L^{-1/3}$ scaling to return, but fig. 4c shows that this does not happen either. The reason is that the Debye screening length is still comparable to the size of the tail for our range of salt concentrations. Thus we find ourselves in a regime where the height of the tail does not obey any particular type of scaling.

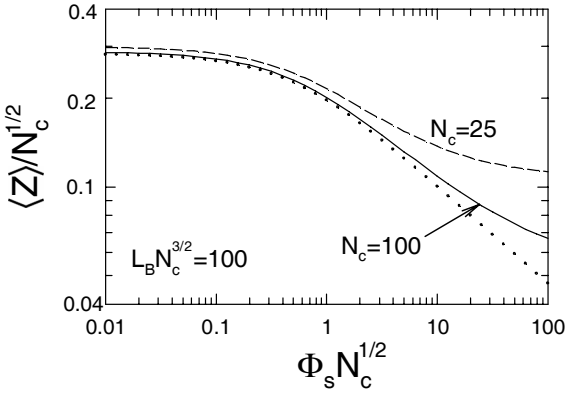

Fig. 5. SCFT prediction for the average segment height of an isolated brush, $\langle Z\rangle$, as a function of salt concentration, Φ_s. The dashed and solid curves are for brushes with $N_c = 25$ and 100 charges per polymer chain, respectively, while the dotted curve shows the SST prediction from fig. 3.

Naturally the depletion zone and the tail both increase the average segment height, $\langle Z\rangle$. This is demonstrated in fig. 5 for brushes with $N_c = 25$ and 100 charges per chain. The deviation away from the SST prediction (dotted curve) is larger for small N_c simply because the fluctuations are more significant, but so much so that the $\Phi_s^{-1/3}$ scaling is lost. The reason is simple. The contraction of the brush occurs because the salt screens the electrostatic interactions causing the field to gradually vanish. In the absence of a field, SST predicts the complete collapse of the brush, whereas the chain fluctuations in SCFT prevent the polymer distribution from contracting below $\langle Z\rangle = 0.543$ [17]. Indeed the dashed curve for $N_c = 25$ plateaus at 0.1086 and similarly the solid curve for $N_c = 100$ approaches 0.0543 in the limit of large Φ_s.

3.3 SST for a compressed brush

Now that the isolated brush is well understood, we turn our attention to the SST treatment of a compressed brush. The solution to the SST is obtained analytically by selecting values for $\Phi_s N_c^{1/2}$, $L/N_c^{1/2}$ and Ψ_L. From these values, f_c is evaluated using eq. (14), and then $L_B N_c^{3/2}$ is calculated from eq. (10). Next Ψ_D is obtained from eq. (18) and lastly $D/N_c^{1/2}$ is evaluated from eq. (19). Of course, it is more natural to work with the independent variables, $L_B N_c^{3/2}$ and $D/N_c^{1/2}$, rather than the dependent quantities, $L/N_c^{1/2}$ and Φ_L. This can be done using a simple Newton-Raphson iteration to adjust $L/N_c^{1/2}$ and Φ_L so as to achieve the desired values of $L_B N_c^{3/2}$ and $D/N_c^{1/2}$.

Figure 6a shows the effect of compressing the polymer profiles from fig. 2 to $D/N_c^{1/2} = 0.6$. The compression of the two thicker brushes for $\Phi_s N_c^{1/2} = 0.0$ and 0.3 has nearly transformed them into the same profile, while the two thinner brushes for $\Phi_s N_c^{1/2} = 1.0$ and 3.0 remain virtually unperturbed. For the higher compression of $D/N_c^{1/2} = 0.4$ in fig. 6b, the three brushes for

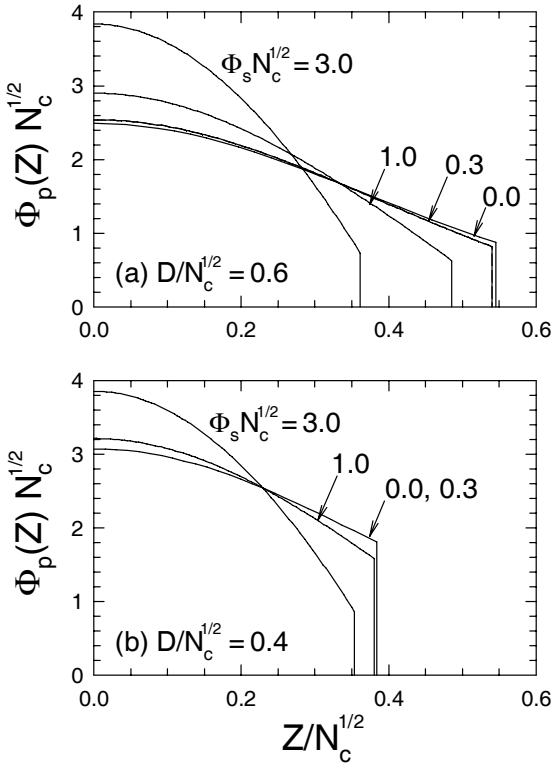

Fig. 6. SST predictions for the polymer profile of a brush, $\Phi_p(Z)$, compressed to (a) $D/N_c^{1/2} = 0.6$ and (b) $D/N_c^{1/2} = 0.4$ plotted for different salt concentrations, Φ_s.

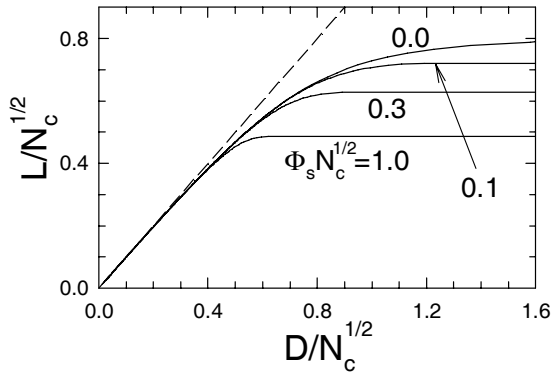

Fig. 7. SST prediction for the height of a compressed brush, L, as a function of separation between the grafting surfaces, $2D$, plotted for different salt concentrations, Φ_s. The dashed line denotes the height of the midplane.

$\Phi_s N_c^{1/2} = 0.0$, 0.3 and 1.0 have now been squeezed towards a common profile, while the one for $\Phi_s N_c^{1/2} = 3.0$ is just beginning to feel the compression. In any case, the most important observation is that the effect of salt appears to vanish under compression.

Figure 7 plots the brush height, L, as a function of the compression, D, for various salt concentrations, Φ_s. The behavior is easily understood. The brush height, L, does not begin to contract until the gap, $2(D - L)$, between the opposing brushes becomes comparable to the

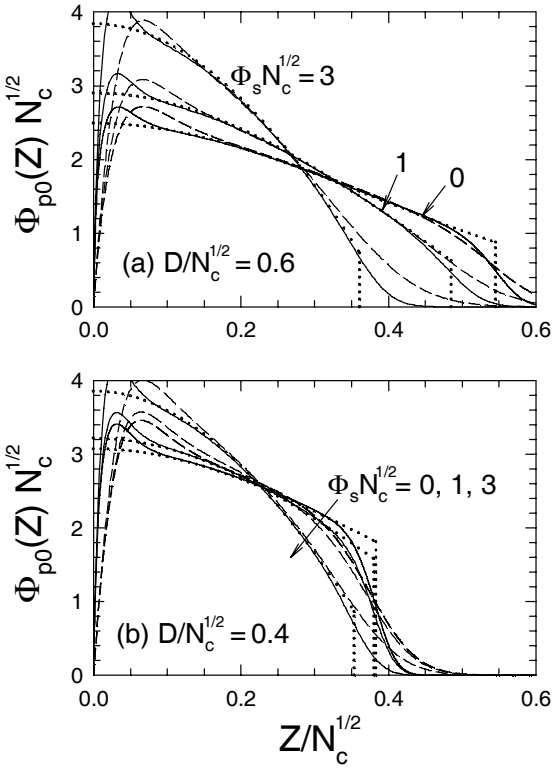

Fig. 8. SCFT predictions for the polymer profile of a single brush, $\Phi_{p0}(Z)$, compressed to (a) $D/N_c^{1/2} = 0.6$ and (b) $D/N_c^{1/2} = 0.4$ plotted for different salt concentrations, Φ_s. The dashed and solid curves are for brushes with $N_c = 25$ and 100 charges per polymer chain, respectively, while the dotted curves show the SST predictions from fig. 6.

Debye screening length, Λ_D, which is the point where the brushes start to feel each other. Once the gap becomes small relative to Λ_D, the screening effect of the salt become irrelevant and the polymer profile converges to the zero-salt limit. Consequently, the previous zero-salt prediction by Zhulina and Borisov [14] that the polymer-free gap remains finite as $D \to 0$ continues to hold regardless of how much salt is added. Of course, if the gap becomes too narrow, it will be destroyed by chain fluctuations.

3.4 SCFT for a compressed brush

The last issue to address is the effect of chain fluctuations on a compressed brush. Figure 8 replots some of the profiles that were previously calculated with SST in fig. 6. Again the SCFT profiles are similar to the SST predictions, apart from the depletion zone and the tail extending beyond L. At the lower compression of fig. 8a, very little of the tail extends beyond D, implying a negligible degree of interpenetration between opposing brushes. The only exception is with $N_c = 25$ and no salt. However, at the higher compression of fig. 8b, SCFT predicts significant interpenetration, apart from the one case where $N_c = 100$ and $\Phi_s N_c^{1/2} = 3$. Evidently, larger values of N_c are desirable because they result in relatively small tails,

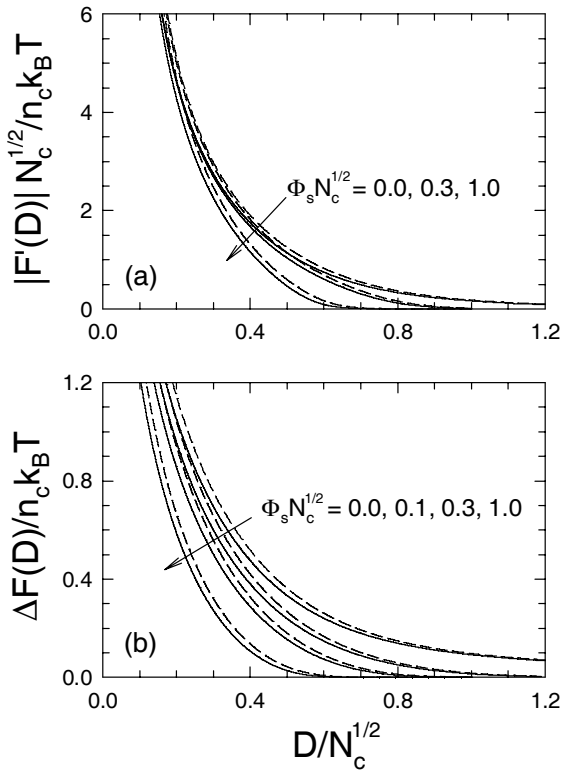

Fig. 9. SCFT prediction for the normal force between (a) parallel plates and (b) crossed cylinders as a function of separation, $2D$.

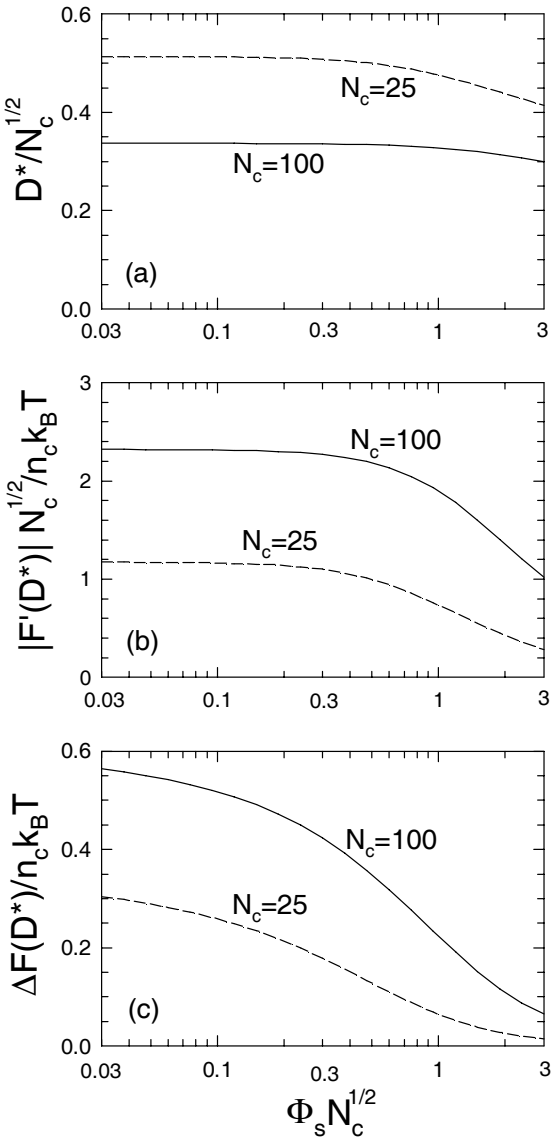

Fig. 10. SCFT prediction for (a) the separation at which the opposing brushes make contact, $2D^*$, and the normal force between (b) parallel plates and (c) crossed cylinders at the point of contact plotted as a function of salt concentration, Φ_s.

and higher values of Φ_s reduce interpenetration by causing the brush to contract.

However, low interpenetration on its own is not enough. It is also important to have a large normal force. Figure 9a shows the normal force between two parallel plates as a function of their separation, $2D$. We have not plotted the SST prediction for the normal force, but it is almost indistinguishable from the SCFT predictions for $N_c = 100$ (solid curves). For the smaller value of $N_c = 25$ (dashed curves), the normal force is noticeably larger than the SST prediction, which is not surprising because the brushes have relatively large tails. The most important observation, though, is that salt reduces the normal force, which could have been anticipated from fig. 2 since it causes the brushes to contract as well as reduces the range of the charge distribution extending beyond the brushes. So with respect to the normal force, small values of N_c and Φ_s are desirable.

For completeness, fig. 9b plots the normal force for the crossed-cylinder geometry. In this case, the addition of salt has a more detrimental effect on the normal force. Still, the general conclusion is that reducing N_c and Φ_s increases the normal force.

Now we sort out the relative importance of the opposing trends where reducing N_c and Φ_s increases the normal force, which is desirable, while also increasing the interpenetration, which is undesirable. To start, we locate the separation, $2D^*$, where significant contact between the brushes first occurs, which is expected to coincide with the onset of sliding friction. Using the same criterion as in our earlier work [17], we define $2D^*$ as the point were 1% of each brush extends beyond the midplane (*i.e.*, $\Sigma_p = 0.01$). Figure 10a plots the point of contact between the brushes, defined in this way, as a function of Φ_s for $N_c = 25$ (dashed curve) and $N_c = 100$ (solid curve). As it turns out, the addition of salt barely reduces the point of contact, until the salted-brush regime (*i.e.*, $\Phi_s N_c^{1/2} \gtrsim 1$). Next fig. 10b plots the normal force between parallel plates at the point of contact, $D = D^*$, as a function of Φ_s. Although added salt reduces the normal force, the effect is again negligible until the salted-brush regime where there is then a sharp drop in force. Figure 10c repeats the calculation, but for crossed cylinders. In this case, the normal force starts dropping off at much lower salt concentrations; the reason will be explained in the next section.

4 Discussion

The present study has examined the impact of salt on the polymer profiles and normal force between two opposing polyelectrolyte brushes using equilibrium theory, extending our earlier study for salt-free conditions [17]. The normal force is derived directly from the free energy using eq. (28) for planar brushes and eq. (29) for crossed cylinders. Although we use an equilibrium theory, these predictions should remain reasonably accurate under shear while the brushes are separated (*i.e.*, $D \gtrsim D^*$). Provided the shear rate and solvent viscosity are not too high, the velocity gradient of the solvent will tend to be confined to the polymer-free gap. Even if the solvent flow does stretch the polymers in the lateral direction, this will not significantly affect behavior in the normal direction provided that the Gaussian chain model remains valid. This is because the stretching energy of a Gaussian chain decouples in the orthogonal directions. Since we are assuming that the onset of sliding friction coincides with the point of physical contact between the brushes (*i.e.*, $D \approx D^*$), the normal forces plotted in fig. 10 represent the maximum loads the brushes can support before the friction becomes significant.

The main consequence of adding salt is to reduce the range of the interaction between the brushes, as demonstrated theoretically in fig. 9a and experimentally by Dunlop *et al.* [4]. The effect is two-fold. Firstly the brush height, ℓ, contracts with increasing salt concentration, ρ_s, and secondly the range of the charge distribution from the free ions extending beyond ℓ is limited by the Debye screening length, $\lambda_{\mathrm{D}} \sim \rho_s^{-1/2}$ (see fig. 2). Nevertheless, as the brushes are squeezed together, the polymer profiles and the normal force between them recover to the salt-free conditions once the gap between the brushes, $2(d-\ell)$, becomes small relative to λ_{D} (see figs. 6 and 8). As a result, the point of physical contact between the brushes (see fig. 10a) and the corresponding normal force (see fig. 10b) are remarkably unaffected by the addition of salt.

The effect of salt on the normal force between crossed cylinders is more significant (see fig. 10c), but this is easily understood. For crossed cylinders, there is a distribution of separations, of which $2d$ is the minimum separation at the center where the cylinders cross. The normal force originates from a finite patch between the cylinders, where the separation is within the range of the interaction. Although, the normal force at the center of the patch, where the separation is smallest, is relatively unaffected by the added salt, the size of the patch becomes smaller due to the fact that the salt reduces the range of the interaction. Even still, the reduction in normal force happens quite gradually and thus the addition of salt is still not particularly detrimental.

The combination of SST and SCFT has proven to be rather powerful. The SST provides valuable analytical results and scaling predictions, which greatly aid our understanding of the system, while SCFT provides the fluctuation corrections necessary to investigate the interpenetration of the brushes. It is particularly nice that both theories apply mean-field theory to the exact same Gaussian chain model [39]. Since the only difference between the theories is that SST ignores fluctuations about the low-energy classical chain trajectories, any difference between the two theories is entirely due to fluctuations. The alternative lattice SCFT of Scheutjens and Fleer [40] applied to this system by Israëls *et al.* [41] uses a different model, making it less straightforward to ascertain the effect of fluctuations. In particular, it would be difficult to extract the fluctuation-induced tails plotted in fig. 4 since L is model dependent.

Unfortunately, exact solutions to the SST are particularly rare. Melt [15] and semi-dilute [16] neutral brushes are the two well-known examples for which the theory can be solved analytically. In these cases, the field, $w(z)$, is parabolic, and in fact it is always guaranteed to be so if $\rho_p(z)$ is a non-increasing function of z [42] as is the case in the present polyelectrolyte system. For melt brushes $\rho_p(z)$ is constant and for semi-dilute neutral brushes $\rho_p(z) \propto w(z)$. Because the polymer profile is known in advance, the theory is readily solved. Similarly, the solution for semi-dilute polyelectrolyte brushes is possible in a theta solvent because $\psi(z) \propto w(z)$, which allows $\rho_p(z)$ to be deduced from the Poisson-Boltzmann equation. As soon as one deviates from a theta solvent, this simplification is lost and one has to resort to numerical solutions [43]. Fortunately, as Pincus [44] argued, the electrostatic interactions generally dominate the effects of solvent quality, and so it is not such a restrictive assumption to neglect the solvent interactions.

Miklavic and Marcelja [45] did examine the interaction between strong (quenched) polyelectrolyte brushes in good solvent conditions, but they had to linearize the Poisson-Boltmann equation to obtain an analytical solution to the SST. Unlike for the theta solvent condition, their opposing brushes came into physical contact under compression, but interestingly they did report some contraction of the brushes preceding physical contact. Unfortunately, they did not investigate the details of this behavior.

Biesheuvel [46] also performed SST calculations for compressed polyelectrolyte brushes allowing for an arbitrary solvent quality, and furthermore he considered both quenched and annealed polyelectrolytes. In that case, he assumed an Alexander-de Gennes box profile for $\rho_p(z)$ and imposed electro-neutrality. The first approximation results in some quantitative inaccuracies, but the second actually has qualitative implications. In particular, it prevents the opposing brushes from interacting with each other prior to physical contact, and hence the contraction of the brushes in fig. 7 is automatically lost.

While the SST becomes difficult to solve without invoking further approximations, the numerical SCFT [27–29] is much more versatile [47–50]. For example, it can readily handle annealed or quenched polyelectrolytes under the full range of solvent qualities from poor to good, and concentrations from semi-dilute up to melts. Below the semi-dilute regime, the mean-field approximation becomes invalid. In situations where N_c is not large enough

to justify smearing the charge uniformly along the polymer backbone, SCFT could handle discrete charges along the polymer chain either regularly or randomly spaced. It could equally well account for finite flexibility and extensibility of the polymer chains [51] as well as polydispersity in the chain length [52,53], which can become rather significant for brushes grown from the grafting surface [4]. Indeed, a whole host of generalizations are possible within the framework of SCFT without resorting to additional approximations.

There have been a couple preliminary studies [2,3] examining the effects of salt on the normal and shear forces of polyelectrolyte brushes, and Giasson *et al.* are currently performing a more comprehensive study. Even the simple versions of SST and SCFT considered here have proven to be remarkably effective at predicting the normal force between neutral brushes [54], and thus it will be interesting to see if they perform similarly well for polyelectrolyte brushes. For neutral brushes, the SST significantly underestimates the normal force, but for charged brushes, the SST should be sufficiently accurate. Likewise, it would be interesting to see if the onset of sliding friction coincides well with the point where physical contact between the brushes is predicted to occur, but this would have to be done with SCFT.

5 Conclusions

We have examined the effect of salt on strong (quenched) polyelectrolyte brushes in a theta solvent using equilibrium statistical mechanics. The assumption of a theta solvent permitted us to obtain an exact analytical solution to the classical strong-stretching theory (SST) introduced by Semenov [15] and by Milner, Witten and Cates [16]. Furthermore, the numerical self-consistent field theory (SCFT) of Edwards allowed us to investigate the effect of chain fluctuations. Because of the large parameter space, we restricted our study to osmotic brushes ($L_B N_c^{3/2} = 100$), where the charge on the polymer chains is well screened by the free ions.

Our study began with a brief look at an isolated brush, which was studied previously by Borizov and Zhulina [23] using SST and by Israëls *et al.* [41] using a lattice version of SCFT. According to the classical SST, low concentrations of salt, ρ_s, cause a mild contraction in the brush height, ℓ, while the high concentrations of the so-called salted-brush regime produce a more rapid decrease of $\ell \sim \rho_s^{-1/3}$. The chain fluctuations included in SCFT produce a depletion zone next to the grafting surface and a tail extending beyond classical brush height, ℓ. This increases the average segment height, and can wipe out the $\ell \sim \rho_s^{-1/3}$ scaling when the fluctuations are particularly large (*e.g.*, $N_c \ll 100$). We also checked to see if the size of the fluctuation-induced tail exhibited either the $\ell^{1/5}$ scaling for salt-free brushes or the conventional $\ell^{-1/3}$ scaling expected for the salted-brush regime, but our study appears to be in an intermediate regime where there is no particular scaling behavior.

The main focus of our investigation was the normal force and interpenetration between opposing brushes compressed to a separation of $2d$ (see fig. 1). The addition of salt tends to eliminate the long-range part of the interaction as previously demonstrated by experiment [4]. This is partly because of the above contraction in ℓ, but mainly because the electrostatic interaction between the brushes is screened when the polymer-free gap separating them, $2(d-\ell)$, exceeds the Debye screening length, $\lambda_D \sim \rho_s^{-1/2}$. Once the brushes start to interact, there is a further contraction in ℓ that tends to maintain the polymer-free gap, allowing the brushes to develop a large normal force without any significant physical contact. Provided ρ_s is below the salted-brush regime, the normal force between parallel brushes recovers to the salt-free value when $2(d-\ell)$ becomes small relative to λ_D. However, some of the normal force is lost between crossed cylinders, because the absence of a long-range interaction reduces the area over which the cylinders interact.

Although our calculations are specific to static equilibrated brushes, our predictions for the polymer profile and normal force should remain relatively accurate under shear up to the point of physical contact between the opposing brushes (*i.e.*, $D \gtrsim D^*$), provided the shear rate and viscosity of the solvent are not too large. Assuming that the onset of sliding friction coincides with the point of physical contact, fig. 10 provides the maximum normal force that the system can support without introducing significant levels of friction. Thus we can expect that the superb lubricative properties observed for salt-free conditions [2–4] will survive the addition of salt, provided one stays clear of the salted-brush regime.

We acknowledge Suzanna Giasson for useful discussions and the EPSRC for financial support (grant no. EP/F068425/1).

References

1. J. Klein, E. Kumacheva, D. Mahalu, D. Perahia, L.J. Fetters, Nature **370**, 634 (1994).
2. U. Raviv, S. Glasson, N. Kampf, J.-F. Gohy, R. Jérôme, J. Klein, Nature **425**, 163 (2003).
3. U. Raviv, S. Giasson, N. Kampf, J.-F. Gohy, R. Jérôme, J. Klein, Langmuir **24**, 8678 (2008).
4. I.E. Dunlop, W.H. Briscoe, S. Titmuss, M.J. Jacobs, V.L. Osborne, S. Edmondson, W.T.S. Huck, J. Klein, J. Phys. Chem. B **113**, 3947 (2009).
5. B. Liberelle, S. Giasson, Langmuir **24**, 1550 (2008).
6. R. Tadmor, J. Janik, J. Klein, L.J. Fetters, Phys. Rev. Lett. **91**, 115503 (2003).
7. J.B. Sokoloff, J. Chem. Phys. **129**, 014901 (2008).
8. A. Galuschko, L. Spirin, T. Kreer, A. Johner, C. Pastorino, J. Wittmer, J. Baschnagel, Langmuir **26**, 6418 (2010).
9. L. Spirin, A. Galuschko, T. Kreer, A. Johner, J. Baschnagel, K. Binder, Eur. Phys. J. E **33**, 307 (2010).
10. Q. Cao, C. Zuo, L. Li, H. He, Modelling Simul. Mater. Sci. Eng. **18**, 075001 (2010).

11. O.J. Hehmeyer, J.M. Stevens, J. Chem. Phys. **122**, 134909 (2005).
12. M. Sirchabesan, S. Giasson, Langmuir **23**, 9713 (2007).
13. C. Ibergay, P. Malfreyt, D.J. Tildesley, Soft Matter **7**, 4900 (2011).
14. E.B. Zhulina, O.V. Borisov, J. Chem. Phys. **107**, 5952 (1997).
15. A.N. Semenov, Sov. Phys. JETP **61**, 733 (1985).
16. S.T. Milner, T.A. Witten, M.E. Cates, Macromolecules **21**, 2610 (1988).
17. M.W. Matsen, Eur. Phys. E J. **34**, 45 (2011).
18. S.F. Edwards, Proc. Phys. Soc. London **85**, 613 (1965).
19. J. Klein, Proc. Inst. Mech. Eng. Part J: J. Eng. Tribol. **220**, 691 (2006).
20. T. Moro, Y. Takatori, K. Ishihara, T. Konno, Y. Takigawa, T. Matsushita, U.-I. Chung, K. Nakamura, H. Kawaguchi, Nat. Mater. **3**, 829 (2004).
21. M.S. Jin, A.J. Grodzinsky, Macromolecules **34**, 8330 (2001).
22. P.-G. de Gennes, *Scaling Concepts in Polymer Physics* (Cornell University Press, Ithaca, 1979) pp. 69–74.
23. E.B. Zhulina, J. Klein Wolterink, O.V. Borisov, Macromolecules **33**, 4945 (2000).
24. B.V. Derjaguin, Kolloid Z. **69**, 155 (1934).
25. N. Israelachvili, *Intermolecular and surface forces*, 2nd edition (Academic Press, London, 1992).
26. J.U. Kim, M.W. Matsen, Macromolecules **41**, 4435 (2008).
27. A.-C. Shi, J. Noolandi, Macromol. Theory Simul. **8**, 214 (1999).
28. Q. Wang, T. Tankashi, G.H. Fredrickson, J. Phys. Chem. B **108**, 6733 (2004).
29. Q. Wang, T. Tankashi, G.H. Fredrickson, J. Phys. Chem. B **109**, 9855 (2005).
30. I.Y. Erukhimovich, A. Johner, J.F. Joanny, Eur. Phys. J. E **27**, 435 (2008).
31. M.W. Matsen, J.U. Kim, A.E. Likhtman, Eur. Phys. J. E **29**, 107 (2009).
32. J.U. Kim, M.W. Matsen, Eur. Phys. J. E **23**, 135 (2007).
33. R.B. Thompson, K.Ø. Rasmussen, T. Lookman, J. Chem. Phys. **120**, 31 (2004).
34. In ref. [23], their control parameters are chosen to be $\varphi_s \equiv 4L_B N_c^2 \Phi_s/3\pi^2$ and $\zeta \equiv H_0/\Lambda$, where $H_0 = (8N_c/3\pi^2)^{1/2} R_0$ and $\Lambda = 2R_0/L_B N_c$.
35. M. Balastre, F. Li, P. Schorr, J.C. Yang, J.W. Mays, M.V. Tirrell, Macromolecules **35**, 9480 (2002).
36. N.A. Kumar, C. Seidel, Macromolecules **38**, 38 (2005).
37. C. Ibergay, P. Malfreyt, D.J. Tildesley, J. Phys. Chem. B **114**, 7274 (2010).
38. S.T. Milner, T.A. Witten, Macromolecules **25**, 5495 (1992).
39. M.W. Matsen, in *Soft Matter*, Vol. 1: *Polymer Melts and Mixtures*, edited by G. Gompper, M. Schick (Wiley-VCH, Weinheim, 2006).
40. J.M.H.M. Scheutjens, G.J. Fleer, J. Phys. Chem. **83**, 1619 (1979).
41. R. Israëls, F.A.M. Leermakers, G.J. Fleer, E.B. Zhulina, Macromolecules **27**, 3249 (1994).
42. R.R. Netz, M. Schick, Macromolecules **31**, 5105 (1998).
43. S. Misra, S. Varanasi, P.P. Varanasi, Macromolecules **22**, 4173 (1989).
44. P. Pincus, Macromolecules **24**, 2912 (1991).
45. S.J. Miklavic, S. Marcelja, J. Phys. Chem. **92**, 6718 (1988).
46. P.M. Biesheuvel, J. Colloid Interface Sci. **275**, 97 (2004).
47. K.N. Witte, Y.-Y. Won, Macromolecules **39**, 7757 (2006).
48. H. Seki, Y.Y. Suzuki, H. Orland, J. Phys. Soc. Jpn. **76**, 104601 (2007).
49. K.N. Witte, Y.-Y. Won, Macromolecules **41**, 2735 (2008).
50. K.N. Witte, S. Kim, Y.-Y. Won, J. Phys. Chem. **113**, 11076 (2009).
51. M. Deng, Y. Jiang, H.J. Liang, J.Z.Y. Chen, Macromolecules **43**, 3455 (2010).
52. S.W. Sides, G.H. Fredrickson, J. Phys. Chem. **121**, 4974 (2004).
53. M.W. Matsen, Eur. Phys. J. E **21**, 199 (2006).
54. J.U. Kim, M.W. Matsen, Macromolecules **42**, 3430 (2009).